ISBN: 978-3-95450-184-7 doi:10.18429/JACoW-IPAC2018-THPMF022

# STUDY OF POSSIBLE BEAM LOSSES AFTER POST-LINAC COLLIMATION AT EUROPEAN XFEL

S. Liu†, W. Decking, DESY, Hamburg, Germany
F. Wolff-Fabris, XFEL.EU, Schenefeld, Germany

*Abstract*

The European XFEL has been operating with the undulator beamline SASE1 and SASE3 since April 2017 and February 2018, respectively. Despite of the fact that the post-linac collimation has collimated the beam halo to ~20 σ level, relative high radiation doses have been measured especially in the diagnostic undulator (DU) section. In order to find the sources of beam losses after post-linac collimation, BDSIM[1] simulations have been performed. In this paper, we will first present the possible losses generated by the wire scanners upstream of the undulators during a scan. The simulation results will be compared with the measured doses along SASE1 and SASE3 undulators. Based on the simulation results, we will estimate the frequency for wire scanner operations. Besides, the simulations with large extension of beam halo hitting the vacuum chamber aperture transition will also be presented. Finally, other possible radiation dose sources will be discussed.

## INTRODUCTION

The European XFEL is designed to be operated with a nominal beam energy of 17.5 GeV at a maximum repetition rate of 27000 bunches/second [1,2]. The maximum beam power that can be generated is more than 500 kW. The high beam power together with the high loss sensitivity of the undulators raises serious radiation damage concern. This concern is a common issue for all high power machines (e.g. LCLS-II, SCLF). Possible radiation damage to the LCLS-II Permanent Magnet has been studied in simulations using FLUKA [3].

At European XFEL, a ~200 m long post-linac collimation (CL) section is designed to collimate the beam halo and dark current before the undulator section [4]. Beam halo distributions after the CL section have been measured using the wire scanners (WS) installed before and after the collimation sections. The measurement results confirmed that the beam halo is collimated to ~20 σ level [5,6]. However, relative high undulator doses have been measured especially in the diagnostic undulator (DU), which is located at the very beginning of the undulator system. Magnetic field degradation higher than 3% is measured for the DU in SASE3 with a total dose of up to 4 kGy [7]. This demagnetization rate is much higher than the values reported before [3].

The possible main sources for the radiation doses are considered to be mis-steered beam, beam halo and/or spontaneous radiation. Besides, the WS can generate many bremsstrahlung photons during the scan, which is another source of radiation that should be controlled. Since the WS generated radiation dose depends only on the beam charge, wire thickness and scan speed [8], it is much easier to simulate and crosscheck with the experiments. Therefore, we will first present the simulation and experimental results of radiation doses caused by wire scans as a benchmark of the simulation code BDSIM [9].

† shan.liu@desy.de

## RADIATION DOSES CAUSED BY WIRE SCANS

At present, there are in total 4 sets of WS installed at the European XFEL, and they are used for beam size and beam halo measurements. On one WS stage there are three tungsten wires (diameter of 50 µm, 30 µm and 20 µm) with the same orientation and two additional crossed wires with an angle of 60° [10].

Beam halo measurements using the WS have been performed in Nov. 2017 using the 2 sets of WS installed after the CL section and upstream of SASE3 as shown in Fig. 1. These measurements also aim at checking the radiation doses accumulated in the undulators during the scan under SASE condition (undulator gaps closed) and w/o SASE delivery (undulator gaps open). The measurements have been performed with 500 pC $e^-$ beam in single bunch mode with 10 Hz repetition rate. The ø 50 µm tungsten wire was used for the measurements to increase the signal level from the beam halo. The scans were performed in the slow scan mode with a delay time of 1 s for data taking, and 10 shots of data were taken at each scan step[2]. The distance between the first WS after the CL section and the SASE1 DU is ~333 m, 10 scans have been performed using this WS with SASE1 undulator gaps closed. In the SASE3 undulator section, the WS are located ~82 m upstream of the DU and 7 scans have been performed with the undulator gaps open (except for the DU, the gap of which is fixed at 12 mm).

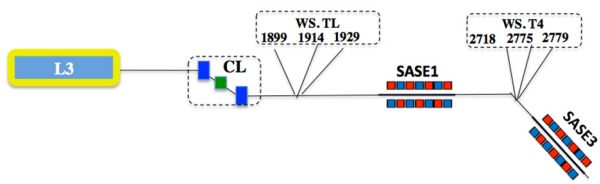


Figure 1: Post-linac beam line layout with WS positions.

A similar setup has been implemented in the BDSIM simulation. Part of the geometries used in the simulation is shown in Fig. 2: a simplified WS station (with one ø 50 µm vertical wire) and two open undulator cells separated by an absorber and a quadrupole.

[1] BDSIM is a toolkit of GEANT4 and it extends the ability of GEANT4 to allow for fast geometry building and fast tracking with design optics.
[2] In normal operation (fast scan mode), the wire moves continuously with a speed adapted to the number of bunches and to the beam size.

ISBN: 978-3-95450-184-7 doi:10.18429/JACoW-IPAC2018-THPMF022

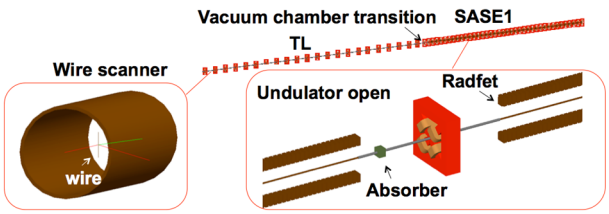


Figure 2: Geometry used in the BDSIM simulation (only the case with open undulators is shown here).

In the simulation, a total number of $10^4$ e$^-$ was generated to hit the wire. The energy losses are recorded downstream of the WS. The energy loss map from WS to the end of SASE1 is shown in Fig. 3. It can be seen that there is a large increase of losses near the entrance of SASE1. Similar increase has been observed at the entrance of SASE3 (not shown here). This is due to the fact that near this location, there are several vacuum chamber aperture transitions: first from ø 40.5 mm to ø 8 mm and then to ø 10 mm followed by the elliptical undulator vacuum chamber, at the end of which there is an absorber with semi-major axis length of 4.5 mm and semi-minor axis length of 4 mm. After the transition points, however, the energy loss starts to decrease.

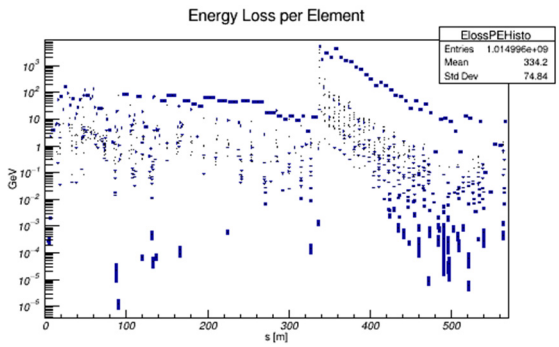


Figure 3: Energy loss per element downstream of the WS (zero position). The vacuum chamber aperture transition starts at ~330 m.

In Fig. 4, one can see the simulated radiation doses[3] both at the Radfet position (blue) and the mean dose for one undulator cell (red). The doses are calculated from the recorded energy losses and normalized according to the real beam charge and total number of bunches that hit the wire during the experiments. In the experiments, the radiation doses are measured using the Radfets, which are installed at the front face of each undulator (one upper and one lower) and they move together with the undulator gap [7]. The doses measured by the upper Radfets along SASE1 and SASE3 are shown in black in Fig. 4 (upper) and (lower), respectively.

[3] Please note that, in the simulation, only electromagnetic processes (G4EmStandardPhysics) are included, i.e. there is no neutron production. Besides, no neutron doses are measured so far at the European XFEL [11].

[4] The increase of doses between cell 20 and cell 30 seems not to be related to the wire scan, but may be caused by the synchrotron radiation generated by the e$^-$ passing through the undulator.

The simulation results agree well with the measurements, especially for the SASE1 case[4]. For the SASE3 case, however, since the undulator gaps are open, the Radfet recorded radiation doses are quite low and fluctuate around zero. It is worth to mention that the Radfet readout at the DU (cell 1 in the plots) location had large fading after a large dose accumulation.

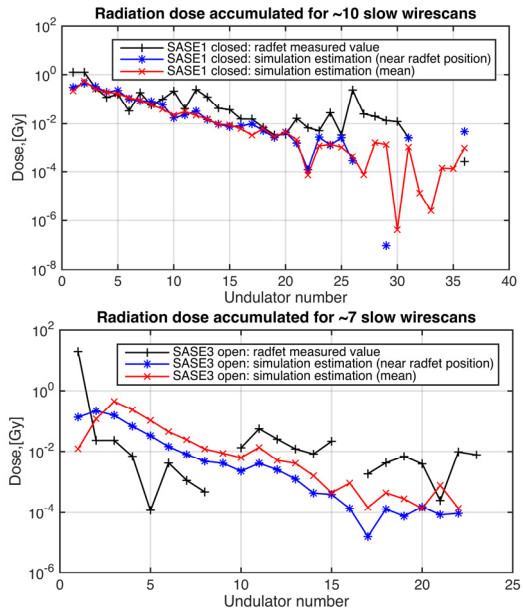


Figure 4: Radiation doses measured by the Radfets during the wire scans in SASE1 (upper) and SASE3 (lower) undulator system (zero and negative values not shown in log-scale).

The maximum doses ($D_{max}$) per continuous scan calculated from the maximum of the measured/simulated for different operation conditions are shown in Table 1. One can see that the maximum dose with SASE1 open is much higher than that with SASE3 open. This can be explained by the typical distance of bremsstrahlung photon impact $L = \frac{R}{\tan\left(\frac{m_e}{E_e}\right)} \approx 548$ m, where $R = 20.25$ mm is the radius of the vacuum chamber, and $E_e$ is the e$^-$ beam energy. Since the WS after the CL section are located much further away to the SASE1 entrance comparing with the WS upstream of SASE3, more photons would hit the vacuum chamber and reach the undulators.

According to $D_{max}$/scan, one can estimate the frequency for the WS operation. The criterion for this estimation is that no more than 0.04% demagnetization occur in 10 years of operation, which corresponds to ~55 Gy/10 years according to the demagnetization rate measured for the DU [7]. The estimated WS operation frequencies are also shown in Table 1.

One should keep in mind that, since the WS are mostly used for emittance measurements and optics matching at the machine set-up phase, the normal operation mode would be with the undulator gaps open. Meanwhile, the WS after the CL sections can be operated with the e-beam dumped in the TLD dump, which is located upstream of SASE1. And some new WS can be installed in

ISBN: 978-3-95450-184-7 doi:10.18429/JACoW-IPAC2018-THPMF022



front of the SASE1 similar to SASE3 case. Therefore, 14 scans/week can be taken as a standard operation frequency for the WS.

Table 1: Estimation of WS Operation Frequency

| Operation conditions | SASE1 open | SASE1 closed | SASE3 open | SASE3 closed |
|---|---|---|---|---|
| $D_{max}$/scan [mGy] | 8.15 | 39.0 | 3.30 | 13.7 |
| $N_{scan}$ /week | 7 | 2 | 14 | 4 |

## BEAM HALO MEASUREMENTS AND SIMULATIONS

It was mentioned before that after the CL section, the beam halo is collimated up to ~20 σ level. Similar measurements have been performed downstream of SASE1 undulators and upstream of SASE3. The measured horizontal beam halo distribution using the first WS downstream of SASE1 (see Fig.1) is shown in Fig. 5. One can see that although the beam shape is far from Gaussian (e.g. due to wakefield, dispersion or optics mismatch), the measurable beam halo is constrained in 20 σ level.

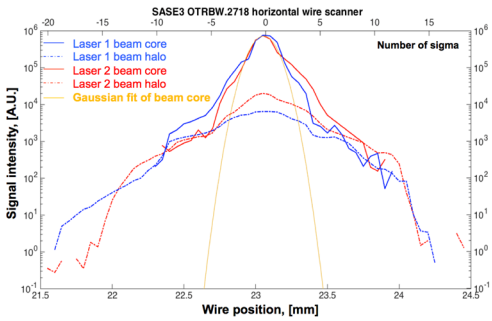


Figure 5: Horizontal beam halo distribution measured upstream of SASE3 for two different injector lasers.

Therefore, with the design optics and perfect orbit, we don't expect that the beam halo can hit the undulator vacuum chamber, which has a physical aperture corresponding to ~100 σ. However, in order to find the correct orbit and get full transmission, during the machine set-up and the undulator beam based alignment (BBA) procedures, the $e^-$ beam is steered frequently before the undulator. The most probable position that the mis-steered beam or beam halo can hit the vacuum chamber would be around the vacuum chamber transition position. Therefore, it is important to estimate the doses that can be generated in these cases. Since it is difficult to predict the incident angle of the mis-steered beam or beam halo, we have generated $10^4$ $e^-$ distributed uniformly in the (x,x',y,y') 4D phase space [12] with the design twiss parameters, but scaled up by factor 530 to fill in the entire vacuum chamber at the entrance of the vacuum chamber transition.

Figure 6 shows the mean radiation dose accumulated at each undulator cell per $e^-$. It can be seen that the DU has the highest dose (one order of magnitude higher than the 1st undulator) as expected. Then the dose decreases slowly along the undulator beam line. This confirms that the high radiation dose and demagnetization of the DU is mainly due to mis-steered beam hitting the vacuum chamber transition. This radiation source has already been controlled by using the Ocelot orbit correction tool [13], which reads the beam positions in a single shot, and then switches the beam off for transfer matrix calculations and orbit corrections. In addition, the slow protection of the beam loss monitors (BLM) [14] in the undulator section can also stop the mis-steered beam in 100 shots.

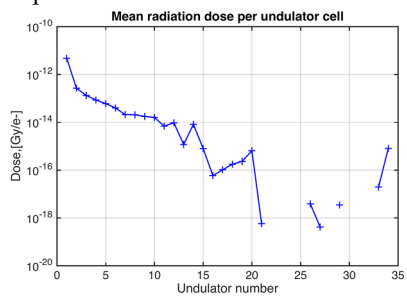


Figure 6: Simulated radiation doses in SASE1 caused by large extension of beam halo hitting the vacuum chamber transition.

## DISCUSSIONS AND PROSPECTS

In the previous sections we have presented the doses caused by the WS and the mis-steered beam/halo. In both cases, we observed the highest dose at the DU followed by a decrease of the doses. During the normal user operation, however, the dose distribution is quite different from the one shown in Fig.6. The measured radiation dose rate per charge rate for different number of bunch operation can be found in Ref. [7]. Except for the relative high doses at the DU and the first undulator (cell #3) (which might be due to the Radfet fading effect), almost no dose is measured before cell #15. However, after cell #15 the doses increases rapidly and reaches maximum at cell #27.

The dose distribution can not be explained by the beam halo hitting the vacuum chamber transition, and since the maximum extension of beam halo measured both upstream and downstream of SASE1 is within 20 σ, the probability of beam halo hitting the undulator vacuum chamber is very small, it can only happen with very large optics mismatch (BMAG>13) or orbit offset (>3mm). Therefore, there are other sources of radiation that are detected by Radfets. One of the most possible sources is the spontaneous synchrotron radiation (SR), which has an opening angle of 1/γ. Ignoring the initial spatial distribution, the length for the point like SR to reach the vacuum chamber is ~110 m, which correspond to ~18 undulators. This rough estimation is very close to the first dose peak at cell #17.

In the future, we will try to put the SR calculated for each cells into BDSIM to simulate the corresponding radiation doses and compare it with the measured values in Ref. [7]. Meanwhile, we will continue the investigation of other beam halo and beam loss generation mechanism, e.g. due to beam-gas scattering, wakefield.

ISBN: 978-3-95450-184-7 doi:10.18429/JACoW-IPAC2018-THPMF022

## ACKNOWLEDGEMENTS

The authors would like to thank the colleagues at DESY and European XFEL: B. Beutner, L. Fröhlich, T. Lensch, D. Nölle, T. Wohlenberg, J. Pflueger, Y. Li for their help in the measurements and fruitful discussions.

## REFERENCES

[1] M. Altarelli, R. Brinkmann *et al.*, "XFEL: The European X-Ray Free-Electron Laser Technical Design Report", DESY, Hamburg, Germany, DESY 2006-097, 2006.

[2] M. Scholz *et al.*, "FEL Performance Achieved at European XFEL", presented at IPAC'18, Vancouver, Canada, Apr.-May 2018, paper MOZGBD2, this conference.

[3] M. Santana-Leitner *et al.*, "Life Expectancy Studies for LCLS-II Permanent Magnet", in Proc. IPAC'17, Copenhagen, Denmark, May 2017, paper TUPAB134, pp. 1640-1642.

[4] V. Balandin, R. Brinkmann, W. Decking, and N. Golubeva, "Optics Solution for the XFEL Post-Linac Collimation Section", DESY, Hamburg, Germany, TESLA-FEL Report 2007-05, 2007.

[5] S. Liu *et al.*, "Beam loss simulations for the implementation of the Hard X-Ray Self-Seeding system at European XFEL", 2017 *J. Phys.: Conf. Ser.* 874 012022

[6] S. Liu *et al.*, "First Beam Halo Measurements using Wire Scanners at the European XFEL", in Proc. of FEL 2017, Santa-Fe, USA, Aug. 2017, paper TUP003.

[7] F. Wolff-Fabris *et al.*, "Status of Radiation Damage on the European XFEL Undulator Systems", presented at IPAC'18, Vancouver, Canada, Apr.-May 2018, paper WEYGBD2, this conference.

[8] J. Welch, "Estimate of Undulator Magnet Damage Due to Beam Finder Wire Measurements", Stanford, CA, USA, Rep. LCLS- TN-06-6, 2006.

[9] I. Agapov *et al.* "BDSIM: A particle tracking code for accelerator beam-line simulations including particle–matter interactions" *Nucl. Instr. Meth. A*, vol. 606(3), pp. 708-712, 2009.

[10] T. Lensch, S. Liu, "Status and Commissioning of the Wire Scanner System for the European XFEL", presented at IPAC'18, Vancouver, Canada, Apr.-May 2018, paper WEPAF047, this conference.

[11] D. Nölle, "XFEL Operation – Radiation Issues", Betriebsseminar Travemünde, Feb. 2018.

[12] R. Yang *et al.*, "Modeling and Experimental Studies of Beam Halo at ATF2", in *Proc. 7th Int. Particle Accelerator Conf. (IPAC'16)*, Busan, South Korea, May 2016, paper MOPMB008, pp. 88-91.

[13] S. Tomin *et al.*, "On-line Optimization of European XFEL with OCELOT", ICALEPCS2017, Barcelona, Spain, doi:10.18429/JACoW-ICALEPCS2017-WEAPL07

[14] T. Wamsat, "Status and Commissioning of the European XFEL Beam Loss Monitor System", presented at IPAC'18, Vancouver, Canada, Apr.-May 2018, paper WEPAF053, this conference.